

Experimental observation of interfacial Rashba-Edelstein magnetoresistance in Cr/YIG heterostructures

Zhendong Chen,¹ Peng Chen,^{2,3} Yifei Wang^④,⁴ Wenqiang Wang,⁵ Zhe Zhang,⁶ Xianyang Lu,⁶ Ronghua Liu,⁵ Xiaolong Fan^④,^{4,*} Guoqiang Yu,^{2,3,*} and Fusheng Ma^{1,*}

¹*Jiangsu Key Laboratory of Opto-Electronic Technology, School of Physics and Technology, Nanjing Normal University, Nanjing 210046, China*


²*Beijing National Laboratory for Condensed Matter Physics, Institute of Physics, Chinese Academy of Sciences, Beijing 100190, China*

³*Songshan Lake Materials Laboratory, Dongguan 523808, China*

⁴*School of Physical Science and Technology, Lanzhou University, Lanzhou 730000, China*

⁵*School of Physics, Nanjing University, Nanjing 210008, China*

⁶*School of Electronic Science and Engineering, Nanjing University, Nanjing 210023, China*

 (Received 12 July 2022; revised 1 December 2022; accepted 22 December 2022; published 10 January 2023)

Interfacial Rashba-type spin-orbit coupling is an attractive effect to provide spin-orbit torques without the presence of heavy metals. In this work, we report the experimental observation of the Rashba-Edelstein magnetoresistance in the Cr/YIG heterostructure, which can indicate the presence of the interfacial spin-orbit coupling. By comparing the angular-dependent magnetoresistance of the Cr/YIG and the Cr/Cu/YIG heterostructures, we identify that the magnetoresistance in the Cr/YIG heterostructure is superimposed with two parts: the Rashba-Edelstein magnetoresistance induced by the interfacial spin-orbit coupling and the anisotropic magnetoresistance induced by the magnetic proximity effect. The Rashba-Edelstein magnetoresistance shows a nonsaturated external field dependence, which can be attributed to the Hanle magnetoresistance and the interfacial antiferromagnetic ordering of the Cr layer. Our findings show an approach to obtain spin-orbit torques via the interfacial spin-orbit coupling for YIG-based devices. Furthermore, our findings also provide an understanding of the multiple couplings at the 3*d*-metal/YIG interface.

DOI: [10.1103/PhysRevB.107.014408](https://doi.org/10.1103/PhysRevB.107.014408)

I. INTRODUCTION

Spin-orbit coupling (SOC) plays a significant role in recent spintronic studies [1–8]. Due to the strong intrinsic SOC in materials such as heavy metals (HMs), the charge currents applied in the materials can be converted to pure spin currents and vice versa, which are known as the spin Hall effect (SHE) and the inverse spin Hall effect (ISHE), respectively [1,3,5,9–11]. Benefiting from these two effects, HMs are main platforms for investigating spin-orbit torques (SOTs), as well as spin current sources and detectors in spintronic devices [6,7,12,13]. In the HM/ferromagnetic (FM) heterostructures, there is a spin Hall magnetoresistance (SMR) which is similar to the anisotropic magnetoresistance (AMR) [14–19]. The physics behind the SMR is the spin current reflection and absorption via SOTs induced by the strong SOC of the HM layers. Thus, the SMR can be a fingerprint of the strong SOC and SOTs in HMs.

Instead of the HMs, the interfacial structures with spatial symmetry breaking can also provide strong Rashba-type SOC, such as the interfaces of metal/metal [20–23], oxide/metal [24–26], oxide/oxide [27,28], and two-dimensional materials heterostructures [29]. This kind of SOC can realize the con-

version between charge currents and pure spin or orbital angular momentum currents with the absence of HMs. These conversion effects are known as Rashba-Edelstein effect (REE) and inverse Rashba-Edelstein effect (IREE) [21–23,26,30], respectively. In the nonmagnetic/ferromagnetic (NM/FM) heterostructures with the interfacial SOC, there will be a Rashba-Edelstein magnetoresistance (REMR) which is similar to the SMR [22,26]. The REMR can also be a fingerprint of the interfacial SOC.

Contrasting with HMs, interfacial SOC of the NM/FM heterostructures can also be an effective provider of SOTs in low-cost spintronic devices. Thus, it is an attractive field to search the NM/FM heterostructures with interfacial SOC. For the 3*d*-metal/YIG heterostructure, there are several works reporting the strong SOC in 3*d*-metal layers [11,31–33]. Recently, the existence of the interfacial SOC at the Cr/YIG interface is experimentally demonstrated by the spin-pumping effect of Cr/YIG and Cr/Cu/YIG multilayers [34]. These studies show a prospect to use 3*d* metals rather than HMs to provide spin currents or SOTs in YIG-based spintronic devices. Although REMR can demonstrate the existence of the interfacial SOC, there are rare works that clearly observe the REMR of the 3*d*-metal/YIG heterostructure. Additionally, it is not clear whether any other interfacial effect exists in the 3*d*-metal/YIG heterostructures except the interfacial SOC. For example, the magnetic proximity effect (MPE) has been observed in several NM/FM heterostructures, and it can

*Corresponding authors: fanxiaolong@lzu.edu.cn; guoqiangyu@iphy.ac.cn; phymafs@njnu.edu.cn

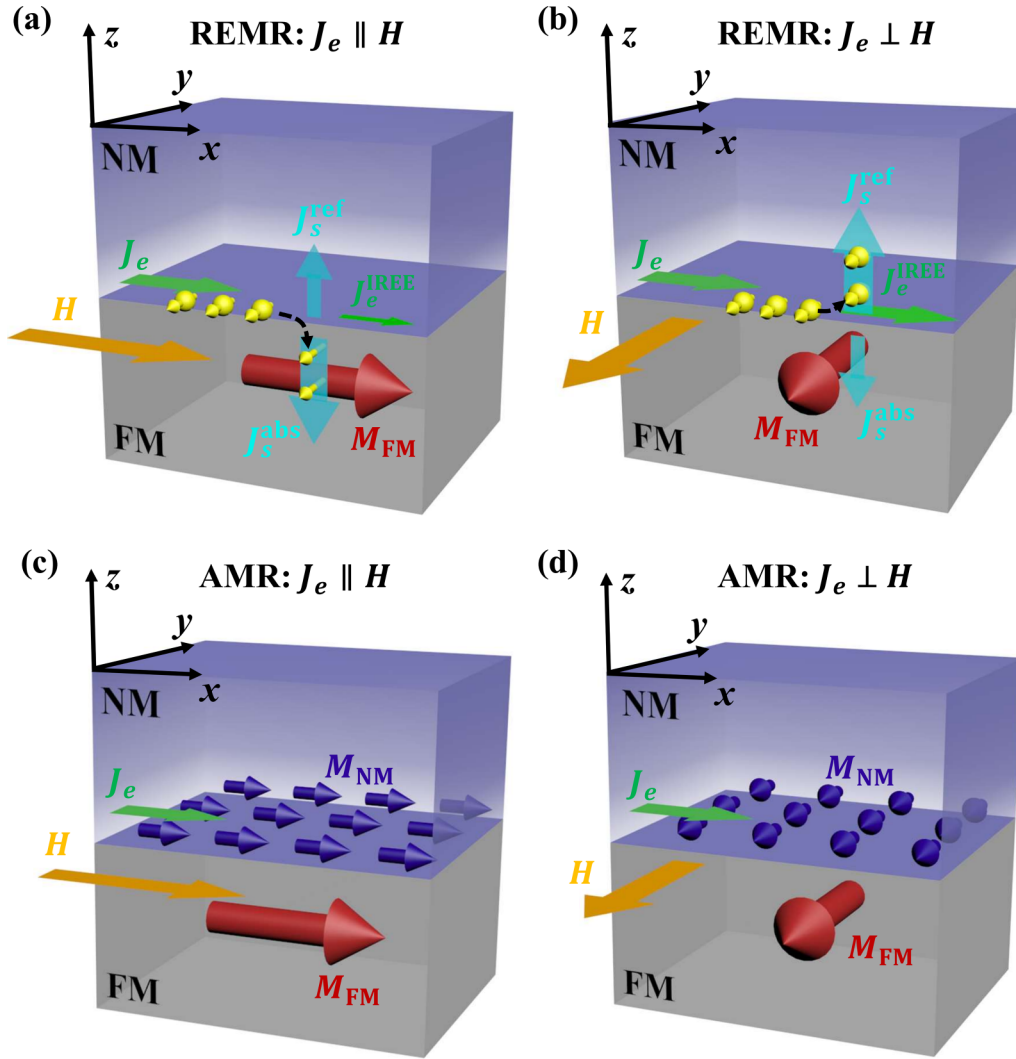


FIG. 1. Sketches of the REMR in the NM/FM heterostructure while (a) $J_e \parallel H$ and (b) $J_e \perp H$. The yellow spheres denote the electrons. The yellow arrows accompanied by the electrons denote the angular moments of the electrons. The red arrows denote the magnetization of the FM layer (M_{FM}). J_s^{abs} and J_s^{ref} are the spin currents which are absorbed and reflected by the FM layer. J_e^{IREE} is the additional charge current induced by the IREE. Sketches of the MPE-induced AMR while (c) $J_e \parallel H$ and (d) $J_e \perp H$. The blue arrows denote the net magnetization of the NM layer at the interface (M_{NM}).

induce magnetic ordering in the NM layers at the interface [35–37]. This interfacial magnetic ordering may also influence the SOT induced by the interfacial SOC.

In this work, we report the experimental observation of the REMR in Cr/YIG heterostructures, which is accompanied by an MPE-induced AMR, although Cr is neither an HM nor a room-temperature FM metal. The REMR and the MPE-induced AMR are identified via analyzing the angular-dependent MR (ADMAR) of the Cr/YIG and the Cr/Cu/YIG heterostructures. The REMR shows a nonsaturated trend under large external fields, which can be attributed to the Hanle MR (HMR) and the influence of the interfacial antiferromagnetic (AFM) ordering of the Cr layer induced by the MPE. Our findings show a prospect to replace HMs by 3d metals in the SOT-driven YIG devices and a further understanding for the complex interfacial couplings between the NM 3d metals and YIG.

II. REMR AND AMR INDUCED BY INTERFACIAL EFFECTS

Both the REMR and MPE-induced AMR in NM/FM heterostructures possess anisotropic spatial symmetries indicated by experimentally measured angular-dependent MR. But their spatial symmetries are different due to their distinct physical mechanisms [22,26,38,39]. Figures 1(a) and 1(b) illustrate the mechanism of REMR [22,26]. When a charge current J_e flows along the x axis at the NM/FM interface with large SOC, a nonzero spin or orbital angular momentum accumulation (AMA) will emerge near the interface with the orientation along the $-y$ axis, which is known as the REE. The AMA can be absorbed or reflected by the FM layer as spin currents J_s^{abs} and J_s^{ref} , respectively. Then, the reflected spin current J_s^{ref} will be accompanied by an additional charge current (J_e^{IREE}) with the same direction to the applied charge current J_e . This spin-to-charge conversion is known as the IREE. The different

strength of J_e^{IREE} will result in an influence of the resistance ratio of the Cr layer, which is defined as the REMR. When $J_e \parallel H$, as shown in Fig. 1(a), the orientation of the AMA at the NM/FM interface is perpendicular to the magnetization of the FM layer M_{FM} . Thus, the AMA will mostly be absorbed by the FM layer; only a weak J_s^{ref} can be reflected by the interface. The weak J_s^{ref} will result in a weak J_e^{IREE} as well as a relatively high resistance ratio. When $J_e \perp H$, as shown in Fig. 1(b), the orientation of the AMA at the NM/FM interface is parallel with M_{FM} . The AMA will be mostly reflected by the interface, and thus results in a strong J_e^{IREE} as well as a relatively low resistance ratio. The REMR possesses an angular dependence of $\sin^2\theta'_M$, where θ'_M is the angle between the orientation of the AMA at the interface and the magnetization of the FM layer. This angular dependence is similar to the angular dependence of the SMR. This similarity is attributed to the similar physical mechanisms of the REMR and the SMR [14,22].

In contrast, the mechanism of MPE-induced AMR in NM/FM heterostructures are shown in Figs. 1(c) and 1(d). It is well known that AMR can be explained by the model of s - d scattering [38,39]. According to this model, the resistance ratio of most FM metals possesses an angular dependence of $\cos^2\theta''_M$, where θ''_M is the angle between the charge current and the magnetization of the FM metal. In the NM/FM heterostructure with the MPE, the magnetic ordering of the NM layer only exists at the interface. Thus, the MPE-induced AMR signal of the NM layer is only provided by the interface. When $J_e \parallel H$, as shown in Fig. 1(c), the NM layer will show a higher resistance ratio due to the AMR effect. And when $J_e \perp H$, as shown in Fig. 1(d), it will show a lower resistance ratio [38,39].

On the one hand, considering that both the REMR and the MPE-induced AMR depend on the interface of the NM/FM heterostructure, they can be investigated by inserting a block layer at the interface between the NM layer and the FM layer. The two kinds of MR should disappear when the inserted layer totally separates the NM and the FM layers. On the other hand, due to the different angular dependences of the REMR and the AMR, they can be distinguished via angular-dependent MR (ADMR) measurements in x - y , x - z , and y - z plane, respectively. To identify the REMR and the AMR of the Cr/YIG heterostructure, we investigate the spatial symmetry of the MR of the Cr/YIG and Cr/Cu(t_{Cu})/YIG ($t_{\text{Cu}} = 0.5, 1, 2, 3$ nm) heterostructures by the ADMR measurements.

III. EXPERIMENTS

The YIG layers in the studied heterostructures are prepared on the GGG(111) substrates by pulsed laser deposition. The crystalline structure, surface morphology, and magnetic properties of the YIG layers are characterized by high-resolved x-ray diffraction, atomic force microscope, and ferromagnetic resonance, respectively. The inserted Cu layers with the thickness of 0.5, 1, 2, and 3 nm, the Cr layers with the thickness of 10 nm, and the Cu capping layer on the top with the thickness of 2 nm are fabricated via magnetron sputtering. Control samples of Pt/Cu/YIG are also fabricated with fixed Pt thickness of 5 nm and various Cu thickness of 0, 0.5, 1, and 2 nm. The ADMR measurements of the Cr/Cu/YIG and Pt/Cu/YIG are

excluded by a PPMS with H rotating in x - y , x - z , and y - z planes. The experiment details and the characterization results are provided in the Supplemental Material [40].

IV. ANGULAR DEPENDENCE OF MR IN CR/YIG HETEROSTRUCTURE

First, we measure the ADMR of Cr/YIG heterostructure at room temperature 300 K with the external field $H = 10\,000$ Oe which rotates in the x - y , x - z , and y - z planes [14,22,26,35]. The measurement sketches are shown in Figs. 2(a)–2(c), and the corresponding measurement results are given in Figs. 2(d)–2(f). We define the MR ratio as $\frac{\Delta R}{R_{90^\circ}} = \frac{R - R_{90^\circ}}{R_{90^\circ}}$, where R is the longitudinal resistance of the device with specific magnetization direction, R_{90° is the longitudinal resistance with φ , θ_{xz} , or θ_{yz} equal to 90° , and ΔR is the difference between these two resistance values. Figure 2(d) obviously shows that the MR ratio in the x - y plane possesses an amplitude of $8.20 (\pm 0.03) \times 10^{-5}$ and an angular dependence of $\frac{\Delta R(\varphi)}{R_{90^\circ}(\varphi)} \sim \cos^2\varphi$. As reported, the AMR, SMR, and REMR all show an angular dependence of $\cos^2\varphi$ in the x - y plane, as shown by the dashed line in Fig. 2(d). In order to identify the MR effects, the angular dependence of the MR ratio in the x - z and y - z planes are also measured. Figure 2(e) shows the angular dependence of MR ratio in the x - z plane. It can be clearly observed that the MR ratio in the x - z plane exhibits an amplitude value of $4.20 (\pm 0.03) \times 10^{-5}$ and an angular dependence as $\frac{\Delta R(\theta_{xz})}{R_{90^\circ}(\theta_{xz})} \sim -\cos^2\theta_{xz}$. This angular dependence conforms to the presence of AMR and thus demonstrates that the Cr layer directly deposited on the YIG layer possesses a magnetic ordering, while the angular dependence of the MR ratio in the y - z plane is shown in Fig. 2(f), which exhibits an amplitude value of $3.80 (\pm 0.04) \times 10^{-5}$ and an angular dependence as $\frac{\Delta R(\theta_{yz})}{R_{90^\circ}(\theta_{yz})} \sim \cos^2\theta_{yz}$. This angular dependence conforms to the presence of both SMR and REMR, and the amplitude is comparable to that of Pt/YIG (in the magnitude of 10^{-4}) [41]. We also measured the SMR of the control sample Pt/YIG with the obtained amplitude of $11.9 (\pm 0.02) \times 10^{-5}$. The MR ratio amplitude of the Cr/YIG heterostructure in the y - z plane is near 1/3 of the value of the Pt/YIG heterostructure and thus reveals that the Cr layer possesses large SOC. Furthermore, it can be found that the amplitude of the MR ratio (the absolute value of the maximum MR ratio) in the x - y plane is approximately equal to the sum of the MR ratio amplitude in the x - z and y - z planes. Therefore, the MR ratio in the x - y plane should be the superposition of the AMR, SMR, and REMR.

V. ANGULAR DEPENDENCE OF MR IN CR/CU/YIG HETEROSTRUCTURES

As shown in Fig. 2, the magnetic ordering and the large SOC of the Cr layer in the Cr/YIG heterostructure can be induced by either the bulk effects of the Cr layer or the interfacial effects. In order to identify the contribution of the bulk effects and the interfacial effects, we investigate the MR ratio of the Cr/Cu(t_{Cu})/YIG heterostructure ($t_{\text{Cu}} = 0.5, 1, 2, \text{ and } 3$ nm) at room temperature as a contrast of the Cr/YIG heterostructure. The MR ratio of the control samples

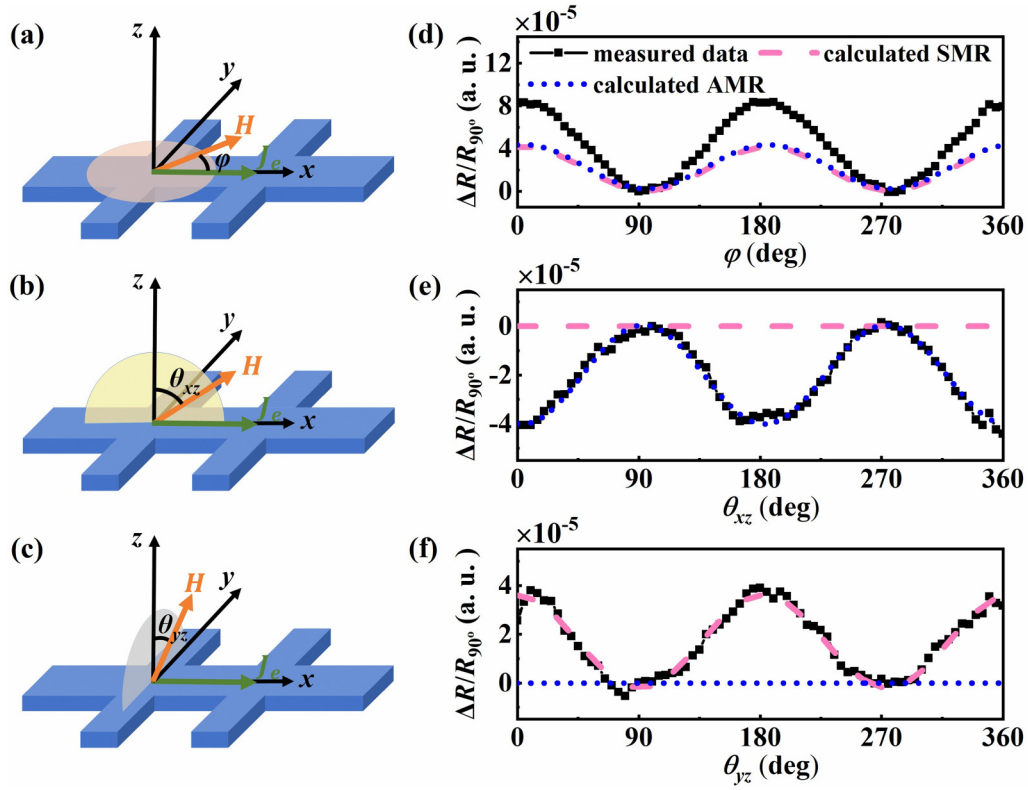


FIG. 2. (a)–(c) Geometric illustrates of the MR measurements of the Cr/YIG heterostructure with the external field H rotating in x - y (a), x - z (b), and y - z (c) plane. φ , θ_{xz} , and θ_{yz} are the azimuth angles of H in x - y , x - z , and y - z planes. The green arrows denote the injected currents J_e . (d)–(f) Angular dependencies of the MR ratio measured in x - y (d), x - z (e), and y - z (f) plane. The pink dashed lines and the blue dotted lines denote the calculated angular dependencies of the SMR (REMR) and the AMR, respectively.

Pt/Cu(t_{Cu})/YIG ($t_{Cu} = 0, 0.5, 1,$ and 2 nm) are also measured. It is well known that Cu is a good conductor of spin currents which cannot block the spin currents induced by the bulk SOC, but can block the interfacial effects [10]. Figure 3(a) shows the MR ratio versus φ of the Cr/Cu(t_{Cu})/YIG heterostructures as well as the control samples of Pt/Cu(t_{Cu})/YIG. It can be easily found that the MR ratio of the Cr/Cu/YIG decreases with t_{Cu} increasing from 0 to 2 nm. With t_{Cu} increasing to 2 nm, the MR ratio decreases to zero simultaneously. In contrast, the MR ratio of Pt/Cu/YIG only shows a decrease of 25% from $11.20 (\pm 0.02) \times 10^{-5}$ to $8.42 (\pm 0.03) \times 10^{-5}$ with t_{Cu} increasing from 0 to 2 nm. Considering the fact that the surface roughness of the YIG layers is ~ 1.2 nm (see Supplemental Material [40]), the interfaces between the Cr (Pt) and YIG layers are totally separated by the Cu layers while $t_{Cu} \geq 2$ nm. Thus, it confirms that both the SMR-like MR effect and the AMR-like MR effect are induced by the interfacial effects at the Cr/YIG interface. The SMR-like magnetoresistance is the REMR which is caused by the REE and IREE at the Cr/YIG interface. The REMR means the existence of a large SOC at the Cr/YIG interface which is caused by the interfacial Rashba effect. This observation agrees with the results of the spin-pumping measurements of the Cr/Cu/YIG heterostructures [34]. Additionally, the AMR-like magnetoresistance can be attributed to the interfacial magnetic ordering of the Cr layer at the Cr/YIG interface, which is induced by the MPE.

It should be noticed that the Cu layers can cause a current shunting effect, which would reduce the current flowing in the Cr layers and the total MR ratio [15]. Meanwhile, the MR ratio may also be reduced by the spin scattering effects caused by the Cu inserted layers and the new interfaces of Cr/Cu and Cu/YIG. These additional scattering effects can make a change of the effective spin mixing conductivity $g_{\uparrow\downarrow}$ between the Cr and YIG layers [11,42,43]. In order to exclude the current shunting effect, we treat the Cr/Cu multilayers as a shunt equivalent circuit as shown in the inset of Fig. 3(b), and analyze the MR ratio in the single Cr layers via Ohm's law. The total resistance of the Cr/Cu multilayers with $\varphi = 90^\circ$ is observed to reduce from 800 to 230 Ohm with t_{Cu} increasing from 0 to 3 nm. This reduction shows that there is an obvious current shunting effect in the Cr/Cu multilayers. By analyzing the current shunting effect via Ohm's law and the equivalent circuit in the inset of Fig. 3(b), we can obtain the MR ratio of the single Cr layers as a function of t_{Cu} . The total MR ratio as a function of t_{Cu} is shown in Fig. 3(b), and as a contrast, the MR ratio of the single Cr layers as a function of t_{Cu} is shown in Fig. 3(c). It can be clearly observed that even though the current shunting effect is considered, the MR ratio of the single Cr layers still shows a trend of reducing to zero with t_{Cu} increasing to 2 nm, which is the same as the total MR ratio. The reduction of the MR ratio of the single Cr layers shown in Fig. 3(c) should not be caused by the current shunting effect. It can only be caused by the block of the interfacial effects or

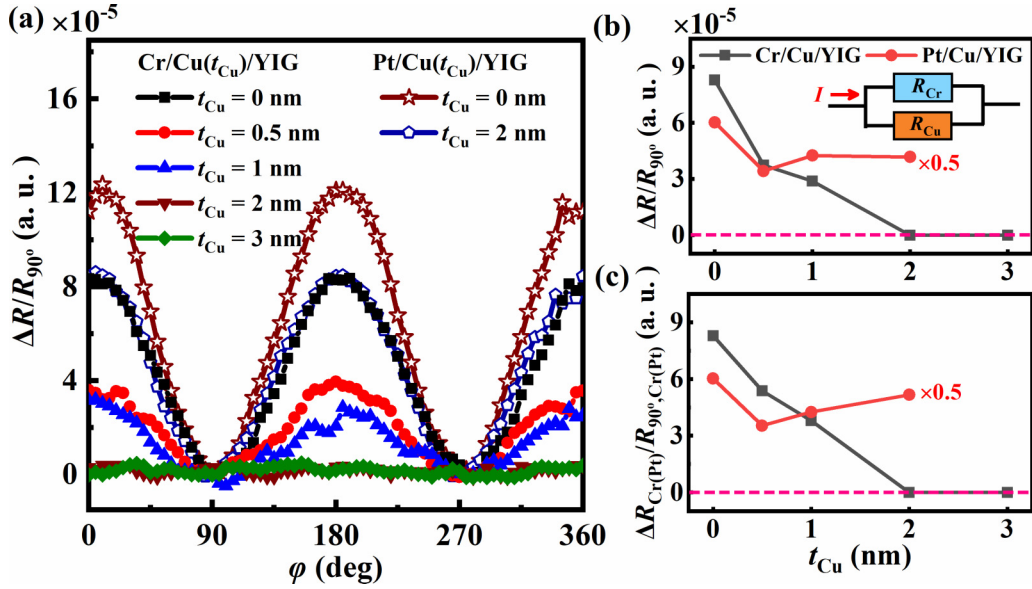


FIG. 3. (a) Dependence of ADMR ratio on ϕ of the Cr/Cu/YIG heterostructures with the Cu thickness $t_{Cu} = 0, 0.5, 1, 2, 3$ nm, and the Pt/Cu/YIG heterostructure with the Cu thickness $t_{Cu} = 0$ and 2 nm. (b) Total ADMR ratio of the Cr/Cu/YIG (black data points) and the Pt/Cu/YIG heterostructures (red data points) as a function of t_{Cu} . The inset is the equivalent circuit of the Cr/Cu/YIG heterostructure. The data of the Pt/Cu/YIG are multiplied by 0.5. (c) ADMR ratio of the single Cr (Pt) layers in the Cr(Pt)/Cu/YIG heterostructures calculated via Ohm's law as a function of t_{Cu} . The data of the Pt/Cu/YIG are multiplied by 0.5.

the spin scattering effect of the Cu layers. In order to exclude the spin scattering effect caused by the Cu layers, we also observe the MR ratio of the Pt/Cu/YIG heterostructures as a function of t_{Cu} in the x - y plane. Pt possesses large intrinsic SOC and thus shows large SMR in Pt/YIG heterostructures as reported in previous works [14,44–47]. The total MR ratio as well as the MR ratio of the single Pt layers in the x - y plane are shown in Figs. 3(b) and 3(c), respectively. It can be found that both the total MR ratio and the MR ratio of the single Pt layers do not exhibit an obviously reducing trend with t_{Cu} increasing. The relatively stable MR ratio of the Pt/Cu/YIG samples demonstrates that the Cu layers and their interfaces cannot cause an obvious spin scattering effect. It agrees with the results of the previous works that Cu is a good conductor of spin currents which shows large spin diffusion length and would not dramatically reduce the $g_{\uparrow\downarrow}$ between the NM and FM layers [11,43,48]. Thus, it suggests that the reduction of the MR ratio with t_{Cu} increasing in Cr/Cu/YIG is not caused by the spin scattering effect of Cu layers. The fact that the Cu inserted layers cannot make an obvious change on $g_{\uparrow\downarrow}$ between the Cr and YIG layers is also demonstrated by the previous works focusing on the spin pumping effect of Cr/Cu/YIG heterostructures. The weak dependence between the Cu inserted layers and $g_{\uparrow\downarrow}$ is demonstrated by the stable damping constant of the Cr/Cu(t_{Cu})/YIG heterostructures with different t_{Cu} [34]. The results of the spin pumping experiments also confirm that the spin-orbit coupling exists at the Cr/YIG interface rather than the interface between the oxidized surface and the Cr layer. This suggestion is demonstrated by the dramatic reduction of the IREE signal intensity while the Cu layer is inserted at the Cr/YIG interface.

VI. FIELD AND TEMPERATURE DEPENDENCE OF MR IN CR/YIG HETEROSTRUCTURE

In order to further understand the interfacial magnetic ordering and the REMR at the Cr/YIG interface, we investigate the ADMR in the x - y , x - z , and y - z planes with H changing from 10 000 to 1000 Oe at room temperature. First, the magnetization hysteresis loops of the Cr/YIG heterostructure is measured in the x - y plane and out of plane by a vibrating sample magnetometer (VSM), as shown in Figs. 4(a) and 4(b), respectively. It reveals that the heterostructure would be saturated under a very low field of near 10 Oe in the x - y plane, and the out-of-plane saturation field along the z axis is ~ 2000 Oe. The saturated magnetization (M_s) of the heterostructure is also obtained to be ~ 196 emu/cm [3] by only considering the volume of the YIG layer. The low coercive field and saturation field in the x - y plane as well as the M_s value conform to the characteristics of YIG which are widely reported [11]. Considering that the magnetic ordering of the Cr layer only exists at the Cr/YIG interface, it is difficult to detect in the VSM measurement. Thus, the measured loop can be regarded as the magnetization loop of the YIG layer. Meanwhile, the MR ratios versus ϕ , θ_{xz} , and θ_{yz} with different H are shown in Figs. 4(c)–4(e). The MR dependence on H in the three planes is directly shown in Fig. 4(f). It can be clearly found in Figs. 4(c) and 4(f) that the MR ratio in the x - y plane dramatically decreases from 8.20×10^{-5} to 0.51×10^{-5} with H decreasing from 10 000 to 1000 Oe, even though all the values of H are much larger than the saturation field of the YIG layer. Figure 4(f) also shows that the MR ratio in the x - y plane possesses a quadraticlike dependence

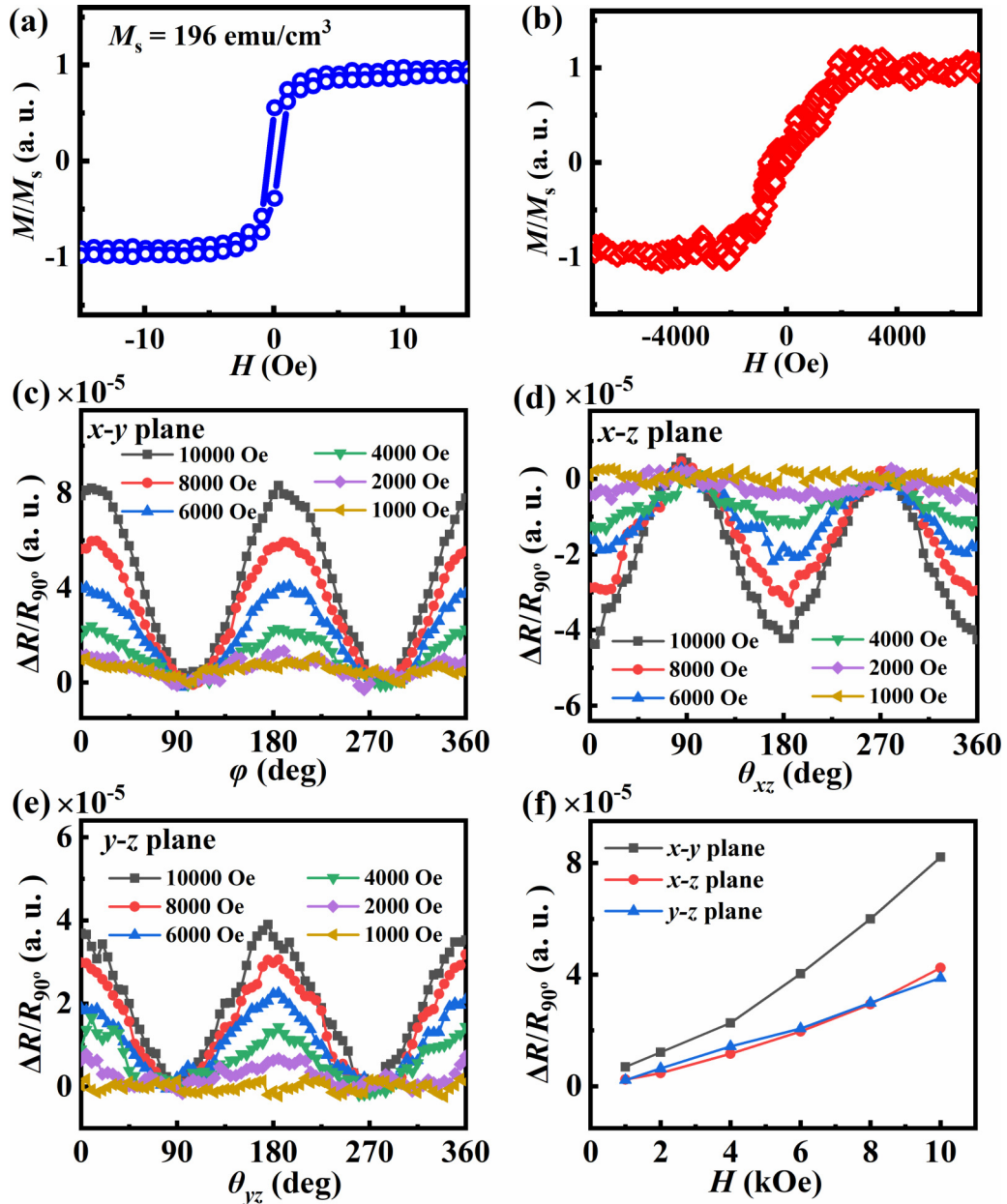


FIG. 4. Magnetization hysteresis loops of the YIG layer in x - y plane (a) and along z axis (b), respectively. (c)–(e) ADMR of the Cr/YIG heterostructure in x - y (c), x - z (d), and y - z (e) plane with different field. (f) Field dependence of the ADMR in x - y , x - z , and y - z planes.

on H . This nonsaturated MR under large H does not agree with that of the HM/FM heterostructures [41] but is similar to that of the HM/AFM heterostructures [49–53]. In order to find out the origin of the nonsaturated MR- H dependence, we also measure the ADMR in the x - z and y - z planes as shown in Figs. 4(d) and 4(e), respectively. For the ADMR in the x - z plane, both Figs. 4(d) and 4(f) show that the MR ratio possesses a nonsaturated dependence on H even though H is larger than 2000 Oe. Since it is well known that the ADMR in the x - z plane is attributed to the pure AMR, the nonsaturated MR- H dependence indicates the nonsaturation of the AMR in the Cr/YIG heterostructure in relatively large H . The nonsaturation can result from the MPE induced AFM ordering in the Cr layer at the Cr/YIG interface [54–56]. The MPE-induced

AFM ordering in the Cr/YIG heterostructure disagrees with the results in the previous work which declared that there is no MPE at the Cr/YIG interface [32]. This difference can be attributed to two factors. On the one hand, the previous work reported in Ref. [32] used anomalous Hall effect (AHE) to demonstrate the existence or absence of the MPE. AHE measurement is an effective method to demonstrate the existence or absence of the MPE-induced FM ordering. However, it is not an effective method to demonstrate the existence or absence of the MPE-induced AFM ordering. This is because of the fact that the AHE voltage of the AFM ordering possesses a quasilinear dependence on the external field, which is similar to that of the ordinary Hall effect voltage [57,58]. On the other hand, the MPE is an interfacial effect and very sensitive

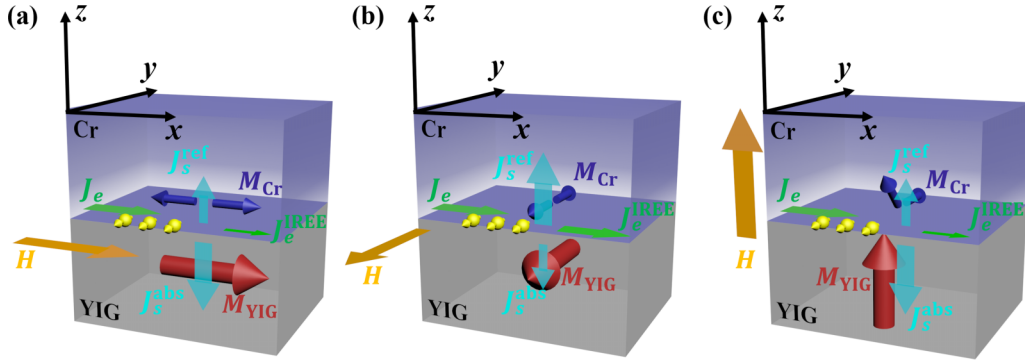


FIG. 5. Sketches of the physical processes of REMR in the Cr/YIG heterostructure with \mathbf{H} along x (a), y (b), and z (c) axis. The red arrows denote the magnetization of the YIG layer, the blue arrows denote the magnetization of the sublattice in the MPE-induced AFM part of the Cr layer.

to the interface status. Thus, different works may produce divided results, i.e., the existence or absence of the MPE in NM/YIG heterostructures, as reported in previous works on Pt/YIG heterostructures [41,59].

For the ADMR measurements in the y - z plane, both Figs. 4(e) and 4(f) show that the MR ratio also possesses a nonsaturated quadraticlike dependence on H with H larger than 2000 Oe. Since the ADMR in the y - z plane is attributed to the pure REMR, it can be noticed that the REMR of Cr/YIG heterostructure is nonsaturated in relatively large H , which does not agree with the SMR results of the HM/FM heterostructures [41]. The nonsaturated REMR can be attributed to two factors: HMR and the reflection and absorption of the AMA caused by the MPE-induced AFM part of the Cr layer at the interface. HMR is induced by the Hanle effect in normal metal layers with large SOC, which means a suppression of the spin accumulation at the interfaces caused by the external field [60,61]. HMR shows a similar angular dependence to that of SMR and REMR, and possesses a quadraticlike increasing dependence on the external field. However, the field-dependent REMR in our work cannot be completely explained by HMR. In the previous works on HMR in NM/FM heterostructures, the MR ratio in the x - y and y - z planes would tend to a specific value which can be seen as the pure SMR when H tends to zero [53,54]. However, in our field-dependent REMR measurements, both the MR ratios in the x - y and y - z planes tend to zero when H tends to zero. Considering that there is an MPE-induced AFM ordering at the interface of the Cr/YIG heterostructure, the REMR can also be influenced by the reflection and absorption of the AMA by the AFM part of the Cr layer at the interface [49–53]. Due to the MPE-induced AFM ordering in the Cr layer, an NM/AFM/FM structure is built near the Cr/YIG interface, just like the Pt/NiO/YIG [45,59], and the AFM part of the Cr layer at the interface will take part in the reflection and absorption of the AMA. When \mathbf{H} is set in the x - y plane, the Néel vector (\mathbf{n}) of the AFM part tends to parallel with \mathbf{H} , and will rotate with \mathbf{H} rotating in the x - y plane [49,50]. When $\mathbf{H} \parallel \mathbf{J}_e$, \mathbf{n} is also parallel with \mathbf{J}_e , thus induces a strong absorption of the AMA, a weak J_e^{IREE} , and a high resistance, as shown in Fig. 5(a). When $\mathbf{H} \perp \mathbf{J}_e$, \mathbf{n} is also perpendicular to \mathbf{H} and thus induces a strong reflection of the AMA, a strong J_e^{IREE} , and a low resistance, as shown in Fig. 5(b). And with \mathbf{H}

increasing, \mathbf{n} of the AFM part will show a stronger tendency to be parallel to \mathbf{H} , thus the REMR caused by the AFM part will increase. Meanwhile, the AMR caused by the AFM part also shows the same angular dependence and field dependence in the x - y plane. Due to the contribution of the AFM part to the REMR and AMR, the MR ratio in the x - y plane possesses a nonsaturated increasing relationship with H , as shown in Figs. 4(c) and 4(f). When \mathbf{H} is in the y - z plane and rotates from the y to z axis, the moments of the AFM part of the Cr layer will partially rotate toward the z axis with \mathbf{H} causing a strong absorption of the AMA and a high resistance, as shown in Fig. 5(c) [49,50]. Considering the reflection and absorption of the AMA by the AFM part of the Cr layer, the REMR caused by the AFM part can be described as [53]

$$\rho_{\text{long}} = \rho_0 + \rho_1 n_y^2, \quad (1)$$

where ρ_{long} , ρ_0 , ρ_1 , and n_y are the longitudinal resistivity ratio, the normal resistivity ratio, the REMR coefficient of the Cr layer, and the projection of \mathbf{n} on the y axis. According to Eq. (1), the REMR caused by the AFM part shows the same angular dependence as the REMR caused by the YIG layer, and shows a nonsaturated increasing dependence on H . It should be noticed that \mathbf{n} can be parallel with or perpendicular to the external field in different AFM materials [49–53]. Thus, the angular dependence of the SMR or REMR in NM/AFM heterostructures can be the same as that in NM/FM heterostructures, or show a 90° shift with respect to NM/FM heterostructures. These two angular dependencies of MR in NM/AFM heterostructures were both observed in previous works. In our work, the angular dependence of the REMR in the Cr/YIG heterostructure is the same as that in NM/FM heterostructures, which demonstrates that \mathbf{n} of the MPE-induced AFM part of the Cr layer tends to parallel with the external field.

To investigate the temperature dependence of the AMR and the REMR effects, we measure the MR ratio in the x - y plane of the Cr/YIG heterostructure with temperature in the range 300–380 K. Figure 6(a) shows the angular-dependent MR ratio under different temperatures. It can be found that the angular dependence and the amplitude of the MR ratio shows a slight reduction with the temperature rising from 300 to 380 K. Figure 6(b) directly shows the MR ratio amplitude versus temperature from 300 to 380 K, which reveals that the

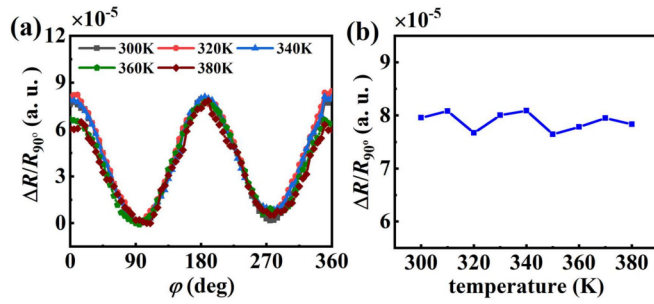


FIG. 6. (a) MR ratio versus ϕ dependences under different temperature changing from 300 to 380 K. (b) Temperature dependence of the MR ratio amplitude in the temperature range 300–380 K.

AMR and the REMR effects of the Cr/YIG heterostructure are not sensitive to temperature in this range. It is known that bulk Cr is an AFM metal with a Néel temperature of ~ 300 K [32], and the Néel temperature should be lower than 300 K for Cr thin film with the thickness in nanometer scale [45,59]. Thus, the stable AMR and REMR of the Cr/YIG heterostructure under temperatures higher than 300 K suggests that the two MRs should not be related to the bulk magnetic ordering of the Cr layer. This also agrees with the above discussion that the magnetic ordering of Cr is caused by the MPE.

Besides, it can be noticed that the interfacial effects in Cr/YIG can also be revealed by the ADMR of various Cr thickness. Meanwhile, the ADMR of various Cr thickness is an effective method to clarify the SOC-dependent parameters such as spin Hall angle θ_{SH} and the spin diffusion length λ_{SD} of Cr [41,49]. In the previous works, the value of θ_{SH} and λ_{SD} of Cr are still a puzzle. In the research of the spin pumping effect in Cr/YIG [31], the researchers declare that θ_{SH} of Cr is equal to -0.051 ± 0.005 which is a half of the value of Pt, and λ_{SD} of Cr is equal to 13.3 nm. In the research of the spin Seebeck effect in Cr/YIG [32], however, the researchers declared that θ_{SH} of Cr is 1/3 of that of Pt, and λ_{SD} of Cr is equal to 2.1 nm. Considering that the MPE, SOC, and spin transfer at the Cr/YIG interface should be sensitive to the interface condition, and both the previous works did not consider the possible existence of the MPE, the dispute on

θ_{SH} and λ_{SD} of Cr can be attributed to the different interface condition and the neglect of the MPE. Thus, θ_{SH} and λ_{SD} of Cr need further study for the ADMR thickness dependence on Cr thickness in the Cr/YIG heterostructure, and should take the interface condition (for example the roughness of the interface [62,63]) and the existence of the MPE into consideration.

VII. CONCLUSION

In summary, we report the observation of the REMR in Cr/YIG heterostructures induced by the interfacial SOC, which is accompanied by an MPE-induced AMR. We find a SMR-like MR effect, as well as an AMR-like MR effect in the Cr/YIG heterostructure, although there is absence of HM with large SOC or room-temperature FM metals in the structure. By comparing the MR ratio of the Cr/YIG and the Cr/Cu/YIG heterostructures, we attribute the two MR effects to the couplings at the Cr/YIG interface: the SMR-like MR effect is attributed to the interfacial REE, and the AMR-like MR effect is attributed to the MPE. Furthermore, the MR ratio shows a nonsaturated trend under large external fields in the x - y , x - z , and y - z planes. It suggests that the MPE induces an AFM ordering in the Cr layer at the interface, which can influence the AMR effect and the reflection of the spin currents. Our findings provide a further understanding of the complex interfacial couplings between the NM 3d metals and YIG, and show a possibility that one can use 3d metals like Cr to provide SOT for YIG-based spintronic devices.

ACKNOWLEDGMENTS

This work was supported by the National Natural Science Foundation of China (Grants No. 12074189, No. 11704191, No. 52171231, No. 12074178, and No. 12104216), the National Key R&D Program of China (Grant No. 2021YFB3601600), the Natural Science Foundation of Jiangsu Province of China (Grant No. BK20200307), and the Postdoctoral Research Funding Program of Jiangsu Province of China (Grant No. 2021K503C).

- [1] J. Sinova, S. O. Valenzuela, J. Wunderlich, C. H. Back, and T. Jungwirth, *Rev. Mod. Phys.* **87**, 1213 (2015).
- [2] A. Manchon, H. C. Koo, J. Nitta, S. M. Frolov, and R. A. Duine, *Nat. Mater.* **14**, 871 (2015).
- [3] X. Qiu, Z. Shi, W. Fan, S. Zhou, and H. Yang, *Adv. Mater.* **30**, 1705699 (2018).
- [4] X.-Y. Feng, Q.-H. Zhang, H.-W. Zhang, Y. Zhang, R. Zhong, B.-W. Lu, J.-W. Cao, and X.-L. Fan, *Chin. Phys. B* **28**, 107105 (2019).
- [5] A. Manchon, J. Železný, I. M. Miron, T. Jungwirth, J. Sinova, A. Thiaville, K. Garello, and P. Gambardella, *Rev. Mod. Phys.* **91**, 035004 (2019).
- [6] C. Song, R. Zhang, L. Liao, Y. Zhou, X. Zhou, R. Chen, Y. You, X. Chen, and F. Pan, *Prog. Mater. Sci.* **118**, 100761 (2021).
- [7] Q. Shao, P. Li, L. Liu, H. Yang, S. Fukami, A. Razavi, H. Wu, K. Wang, F. Freimuth, Y. Mokrousov, M. D. Stiles, S. Emori, A. Hoffmann, J. Akerman, K. Roy, J. P. Wang, S. H. Yang, K. Garello, and W. Zhang, *IEEE Trans. Magn.* **57**, 800439 (2021).
- [8] C. O. Avci, A. Quindeau, C. F. Pai, M. Mann, L. Caretta, A. S. Tang, M. C. Onbasli, C. A. Ross, and G. S. D. Beach, *Nat. Mater.* **16**, 309 (2017).
- [9] O. Mosendz, V. Vlaminck, J. E. Pearson, F. Y. Fradin, G. E. W. Bauer, S. D. Bader, and A. Hoffmann, *Phys. Rev. B* **82**, 214403 (2010).
- [10] C. Hahn, G. de Loubens, M. Viret, O. Klein, V. V. Naletov, and J. Ben Youssef, *Phys. Rev. Lett.* **111**, 217204 (2013).
- [11] F. Yang and P. Chris Hammel, *J. Phys. D: Appl. Phys.* **51**, 253001 (2018).

- [12] T. Jungwirth, J. Wunderlich, and K. Olejník, *Nat. Mater.* **11**, 382 (2012).
- [13] H. Wu, L. Huang, C. Fang, B. S. Yang, C. H. Wan, G. Q. Yu, J. F. Feng, H. X. Wei, and X. F. Han, *Phys. Rev. Lett.* **120**, 097205 (2018).
- [14] H. Nakayama, M. Althammer, Y. T. Chen, K. Uchida, Y. Kajiwara, D. Kikuchi, T. Ohtani, S. Geprägs, M. Opel, S. Takahashi, R. Gross, G. E. W. Bauer, S. T. B. Goennenwein, and E. Saitoh, *Phys. Rev. Lett.* **110**, 206601 (2013).
- [15] J. Kim, P. Sheng, S. Takahashi, S. Mitani, and M. Hayashi, *Phys. Rev. Lett.* **116**, 097201 (2016).
- [16] Y. T. Chen, S. Takahashi, H. Nakayama, M. Althammer, S. T. B. Goennenwein, E. Saitoh, and G. E. W. Bauer, *Phys. Rev. B* **87**, 144411 (2013).
- [17] C. O. Avci, K. Garello, A. Ghosh, M. Gabureac, S. F. Alvarado, and P. Gambardella, *Nat. Phys.* **11**, 570 (2015).
- [18] G. Liu, X. G. Wang, Z. Z. Luan, L. F. Zhou, S. Y. Xia, B. Yang, Y. Z. Tian, G. H. Guo, J. Du, and D. Wu, *Phys. Rev. Lett.* **127**, 207206 (2021).
- [19] L. Zhou, H. Song, K. Liu, Z. Luan, P. Wang, L. Sun, S. Jiang, H. Xiang, Y. Chen, J. Du, H. Ding, K. Xia, J. Xiao, and D. Wu, *Sci. Adv.* **4**, eaao3318 (2018).
- [20] J. C. R. Sánchez, L. Vila, G. Desfonds, S. Gambarelli, J. P. Attané, J. M. De Teresa, C. Magén, and A. Fert, *Nat. Commun.* **4**, 2944 (2013).
- [21] S. Sangiao, J. M. De Teresa, L. Morellon, I. Lucas, M. C. Martinez-Velarte, and M. Viret, *Appl. Phys. Lett.* **106**, 172403 (2015).
- [22] H. Nakayama, Y. Kanno, H. An, T. Tashiro, S. Haku, A. Nomura, and K. Ando, *Phys. Rev. Lett.* **117**, 116602 (2016).
- [23] S. Karube, N. Tezuka, M. Kohda, and J. Nitta, *Phys. Rev. Appl.* **13**, 024009 (2020).
- [24] S. Emori, T. Nan, A. M. Belkessam, X. Wang, A. D. Matyushov, C. J. Babroski, Y. Gao, H. Lin, and N. X. Sun, *Phys. Rev. B* **93**, 180402(R) (2016).
- [25] H. An, Y. Kageyama, Y. Kanno, N. Enishi, and K. Ando, *Nat. Commun.* **7**, 13069 (2016).
- [26] S. Ding, Z. Liang, D. Go, C. Yun, M. Xue, Z. Liu, S. Becker, W. Yang, H. Du, C. Wang, Y. Yang, G. Jakob, M. Kläui, Y. Mokrousov, and J. Yang, *Phys. Rev. Lett.* **128**, 067201 (2022).
- [27] Y. Wang, R. Ramaswamy, M. Motapothula, K. Narayanapillai, D. Zhu, J. Yu, T. Venkatesan, and H. Yang, *Nano Lett.* **17**, 7659 (2017).
- [28] Q. Song, H. Zhang, T. Su, W. Yuan, Y. Chen, W. Xing, J. Shi, J. Sun, and W. Han, *Sci. Adv.* **3**, e1602312 (2017).
- [29] W. Tang, H. Liu, Z. Li, A. Pan, and Y. J. Zeng, *Adv. Sci.* **8**, 2100847 (2021).
- [30] V. M. Edelstein, *Solid State Commun.* **73**, 233 (1990).
- [31] C. Du, H. Wang, F. Yang, and P. C. Hammel, *Phys. Rev. B* **90**, 140407(R) (2014).
- [32] D. Qu, S. Y. Huang, and C. L. Chien, *Phys. Rev. B* **92**, 020418(R) (2015).
- [33] L. Ma, L. Lang, J. Kim, Z. Yuan, R. Wu, S. Zhou, and X. Qiu, *Phys. Rev. B* **98**, 224424 (2018).
- [34] L. Ni, Z. Chen, X. Lu, Y. Yan, L. Jin, J. Zhou, W. Yue, Z. Zhang, L. Zhang, W. Wang, Y. L. Wang, X. Ruan, W. Liu, L. He, R. Zhang, H. Zhang, B. Liu, R. Liu, H. Meng, and Y. Xu, *Appl. Phys. Lett.* **117**, 112402 (2020).
- [35] X. Zhou, L. Ma, Z. Shi, W. J. Fan, J. G. Zheng, R. F. L. Evans, and S. M. Zhou, *Phys. Rev. B* **92**, 060402(R) (2015).
- [36] T. Kuschel, C. Klewe, J. M. Schmalhorst, F. Bertram, O. Kuschel, T. Schemme, J. Wollschläger, S. Francoual, J. Stremper, A. Gupta, M. Meinert, G. Götz, D. Meier, and G. Reiss, *Phys. Rev. Lett.* **115**, 097401 (2015).
- [37] M. Caminale, A. Ghosh, S. Auffret, U. Ebels, K. Ollefs, F. Wilhelm, A. Rogalev, and W. E. Bailey, *Phys. Rev. B* **94**, 014414 (2016).
- [38] A. P. Malozemoff, *Phys. Rev. B* **32**, 6080 (1985).
- [39] S. Kokado, M. Tsunoda, K. Harigaya, and A. Sakuma, *J. Phys. Soc. Jpn.* **81**, 024705 (2012).
- [40] See Supplemental Material at <http://link.aps.org/supplemental/10.1103/PhysRevB.107.014408> for the detailed information of the sample fabrication and characterization.
- [41] M. Althammer, S. Meyer, H. Nakayama, M. Schreier, S. Altmannshofer, M. Weiler, H. Huebl, S. Geprägs, M. Opel, R. Gross, D. Meier, C. Klewe, T. Kuschel, J. M. Schmalhorst, G. Reiss, L. Shen, A. Gupta, Y. T. Chen, G. E. W. Bauer, E. Saitoh, and S. T. B. Goennenwein, *Phys. Rev. B* **87**, 224401 (2013).
- [42] Y. Sun, H. Chang, M. Kabatek, Y. Y. Song, Z. Wang, M. Jantz, W. Schneider, M. Wu, E. Montoya, B. Kardasz, B. Heinrich, S. G. E. Te Velthuis, H. Schultheiss, and A. Hoffmann, *Phys. Rev. Lett.* **111**, 106601 (2013).
- [43] C. Du, H. Wang, F. Yang, and P. C. Hammel, *Phys. Rev. Appl.* **1**, 044004 (2014).
- [44] H. Shi, Y. Su, Y. Meng, L. Wang, X. Cao, and H. Zhao, *Appl. Phys. Lett.* **119**, 222404 (2021).
- [45] D. Hou, Z. Qiu, J. Barker, K. Sato, K. Yamamoto, S. Vélez, J. M. Gomez-Perez, L. E. Hueso, F. Casanova, and E. Saitoh, *Phys. Rev. Lett.* **118**, 147202 (2017).
- [46] K. I. Uchida, Z. Qiu, T. Kikkawa, R. Iguchi, and E. Saitoh, *Appl. Phys. Lett.* **106**, 052405 (2015).
- [47] S. R. Marmion, M. Ali, M. McLaren, D. A. Williams, and B. J. Hickey, *Phys. Rev. B* **89**, 220404(R) (2014).
- [48] H. L. Wang, C. H. Du, Y. Pu, R. Adur, P. C. Hammel, and F. Y. Yang, *Phys. Rev. Lett.* **112**, 197201 (2014).
- [49] J. H. Han, C. Song, F. Li, Y. Y. Wang, G. Y. Wang, Q. H. Yang, and F. Pan, *Phys. Rev. B* **90**, 144431 (2014).
- [50] Y. Ji, J. Miao, K. K. Meng, Z. Y. Ren, B. W. Dong, X. G. Xu, Y. Wu, and Y. Jiang, *Appl. Phys. Lett.* **110**, 262401 (2017).
- [51] J. Fischer, M. Althammer, N. Vlietstra, H. Huebl, S. T. B. Goennenwein, R. Gross, S. Geprägs, and M. Opel, *Phys. Rev. Appl.* **13**, 014019 (2020).
- [52] L. Baldrati, A. Ross, T. Niizeki, C. Schneider, R. Ramos, J. Cramer, O. Gomonay, M. Filianina, T. Savchenko, D. Heinze, A. Kleibert, E. Saitoh, J. Sinova, and M. Kläui, *Phys. Rev. B* **98**, 024422 (2018).
- [53] J. Fischer, O. Gomonay, R. Schlitz, K. Ganzhorn, N. Vlietstra, M. Althammer, H. Huebl, M. Opel, R. Gross, S. T. B. Goennenwein, and S. Geprägs, *Phys. Rev. B* **97**, 014417 (2018).
- [54] M. Wang, C. Andrews, S. Reimers, O. J. Amin, P. Wadley, R. P. Champion, S. F. Poole, J. Felton, K. W. Edmonds, B. L. Gallagher, A. W. Rushforth, O. Makarovskiy, K. Gas, M. Sawicki, D. Kriegner, J. Zubáč, K. Olejník, V. Novák, T. Jungwirth, M. Shahrokhand *et al.*, *Phys. Rev. B* **101**, 094429 (2020).
- [55] J. Wu, M. H. Karigerasi, D. P. Shoemaker, V. O. Lorenz, and D. G. Cahill, *Phys. Rev. Appl.* **15**, 054038 (2021).
- [56] D. Kriegner, K. Výborný, K. Olejník, H. Reichlová, V. Novák, X. Martí, J. Gazquez, V. Saidl, P. Němec, V. V. Volobuev, G.

- Springholz, V. Holý, and T. Jungwirth, *Nat. Commun.* **7**, 11623 (2016).
- [57] L. Šmejkal, A. H. MacDonald, J. Sinova, S. Nakatsuji, and T. Jungwirth, *Nat. Rev. Mater.* **7**, 482 (2022).
- [58] T. Suzuki, R. Chisnell, A. Devarakonda, Y. T. Liu, W. Feng, D. Xiao, J. W. Lynn, and J. G. Checkelsky, *Nat. Phys.* **12**, 1119 (2016).
- [59] T. Shang, Q. F. Zhan, H. L. Yang, Z. H. Zuo, Y. L. Xie, L. P. Liu, S. L. Zhang, Y. Zhang, H. H. Li, B. M. Wang, Y. H. Wu, S. Zhang, and R. W. Li, *Appl. Phys. Lett.* **109**, 032410 (2016).
- [60] S. Vélez, V. N. Golovach, A. Bedoya-Pinto, M. Isasa, E. Sagasta, M. Abadia, C. Rogero, L. E. Hueso, F. S. Bergeret, and F. Casanova, *Phys. Rev. Lett.* **116**, 016603 (2016).
- [61] H. Wu, X. Zhang, C. H. Wan, B. S. Tao, L. Huang, W. J. Kong, and X. F. Han, *Phys. Rev. B* **94**, 174407 (2016).
- [62] L. Jin, K. Jia, D. Zhang, B. Liu, H. Meng, X. Tang, Z. Zhong, and H. Zhang, *ACS Appl. Mater. Interfaces* **11**, 35458 (2019).
- [63] K. Fukushima, K. Ueda, N. Moriuchi, T. Kida, M. Hagiwara, and J. Matsuno, *Appl. Phys. Lett.* **121**, 232403 (2022).